ROCKET-SPACE DEVICE ENGINEERING AND INFORMATION SYSTEMS
Vol. 6, Iss. 2, 2019, pp. 61–70

Algorithm to Analyze Spectral Characteristics of Snow and Cloud Cover Based on MSU-MR/Meteor-M No. 2 Data

K.I. Zubkova, *contact@spacecorp.ru*
Joint Stock Company "Russian Space Systems", Moscow, Russian Federation
L.A. Grishantseva, *Cand. Sci. (Phys.-Math.), contact@spacecorp.ru*
Joint Stock Company "Russian Space Systems", Moscow, Russian Federation
T.G. Kurevleva, *contact@spacecorp.ru*
Joint Stock Company "Russian Space Systems", Moscow, Russian Federation
A.A. Skripchuk, *contact@spacecorp.ru*
Joint Stock Company "Russian Space Systems", Moscow, Russian Federation
A.A. Morozov, *contact@spacecorp.ru*
Joint Stock Company "Russian Space Systems", Moscow, Russian Federation

Abstract. Prompt acquisition of up-to-date weather data, particularly in the form of snow cover maps and cloud maps, is one of the components providing information support for target use of the orbital remote sensing spacecraft constellation. The planning complex, in addition to weather forecast calculation facilities, is currently equipped with an information database containing MSU-MR/Meteor-M No. 2 images (Gorbunov et al. 2015) in the form of composite images in three shortwave channels (with no theme-based processing). In case the data is insufficient for making decisions, then an operator additionally analyses the data from foreign satellites not included in the planning complex. Performance optimization calls for the automation of weather support processes. The paper proposes an algorithm of generating a snow cover mask and cloud mask using domestic MSU-MR/Meteor-M No. 2 data. The algorithm is based on the spectral characteristics analysis of different types of underlying surface: ground, clouds, and snow. The algorithm uses the reflectance values in channel 1 of MSU-MR (green, 0.63 μm) and in channel 3 of MSU-MR (SWIR, 1.7 μm). The proposed algorithm differs from its foreign counterparts: it employs threshold values dependent on the values of reflectance in channels 1 and 3 rather than constant thresholds. The algorithm was verified across 459 survey routes. Testing confirmed the versatility of the proposed algorithm: thresholds do not depend either on geographical location or on seasons. Considering the continuity of imagery from MSU-MR, this algorithm is capable of producing snow cover and cloud maps that are automatically updated with a periodicity of 2-3 days. This will enable the planning complex to be provided with up-to-date snow cover data.
In the nearest future, the creation of the program module realizing this algorithm and the validation of the possibility of its practical application using means of the simulation stand created within the R&D "Earth remote sensing operator" is planned.

Keywords: remote sensing, snow cover, cloud cover, MSU-MR, Meteor-M

Introduction

One of the directions of modernization of the ground-based and space-based infrastructure of Earth remote sensing (ERS) of priority within the framework of the implementation of measures of the Federal Space Program for 2016-2025 is the automation of technologies of the target use of the orbital constellation (OC) of ERS spacecraft (SC).

The process of target use includes such stages of working with ERS data as the generation of an order for satellite imagery, survey planning, reception of satellite information, its standard and thematic processing as well as the issue of the final product to the customer. Planning a survey session is one of the more resource-intensive aspects of target use.

One of the important constituents of comprehensive planning of satellite surveys is meteorological support. The main purpose of weather forecasting is to assist in deciding on the appropriateness of planning a survey at a given location at a given time as well as in determining the input parameters for exposure calculations. In particular, the presence or absence of snow cover significantly affects the estimate of the time required for accumulating the signal on the planned survey route.

The operators of the planning service use RGB composites of satellite images in the form of global coverages generated at short intervals – ranging from one to two-three days. Currently, the planning complex includes the image of global coverage based on the data from the MSU-MR/Meteor-M No. 2 [1] in the daytime. Contours of the routes being planned are superimposed on the RGB images of the MSU-MR. Additional products involved in the process of assessing the presence of snow cover at the survey location are the snow cover mask provided by data from the AVHRR/MetOp-A, B [2] and daily RGB composites of MODIS images in channels 1-4-3 [3]. The operator makes a decision about the presence or absence of snow cover and/or cloudiness after conducting a visual analysis of the global images at the location of the planned survey. However, the processing of one route is time-consuming (up to several minutes). This significantly slows down the operating process (especially in conditions of a large number of orders) and increases the complexity.

The ultimate goal of working with MSU-MR data is automated generation of regularly updated masks of the snow and cloud covers, directly built into the planning complex. At this stage, an algorithm for the formation of such a mask using MSU-MR/Meteor-M No. 2 has already been created and validated.

The basis for the discrimination of snow and clouds from other types of underlying surfaces are the spectral properties of these objects. Snow and clouds are characterized by elevated values of reflectance (R-values; spectral brightness coefficient) in the visible and near IR-ranges [4-7], by a significant decrease of the reflectance in the short-wave IR-range (SWIR – Short-Wave Infra-Red) and by low values of the radiation temperature in the far IR-range (LWIR — Long-Wave Infra-Red). In the MSU-MR, channel 1 (green 0.6 μm) operates in the visible range; channel 2 (0.8 μm) operates in the near IR-range, channel 3 (1.7 μm) – in the SWIR-1 range; channel 4 (3.8 μm) – in the SWIR-2 range; two channels operate in the far IR-range, which are channels 5 (11 μm) and 6 (12 μm).

Snow and clouds are distinguished reliably from other objects by the contrast of brightness (reflectance) in the visible and near IR-ranges. Nevertheless, the task of separating these objects from each other cannot be fulfilled without resorting to the use of SWIR-range data. In the channels of the visible and near IR-ranges, the R-values of snow and clouds are very close, whereas in channels of the SWIR-range there is a contrast between the R-values of these objects [4, 5]. It is this feature that is used for calculating the NDSI snow index (Normalized Difference Snow Index): NDSI = (Green–SWIR-1)/(Green + + SWIR-1) [8]. Yet, it should be taken into consideration that the use of the NDSI threshold value does not guarantee an unequivocal differentiation between snow and clouds. High values of the NDSI may correspond not only to snow-covered areas but also to so-called ice clouds. The final decision on the type of underlying surface is made after comparing the values of the radiation temperatures in the 11 μm channel with the model average climatic values: if the difference of temperatures significantly differs from 0 K, then the object is considered to be a snow cloud.

In [6], a threshold algorithm for singling out snow according to AVHRR data is given. A block diagram of the algorithm is shown in Figure 1.

The following constant threshold values are used in the algorithm: radiation temperature in channel 4 T4, difference in radiation temperatures in channels 4 and 5 T45, NDVI [9], difference in temperatures in channels

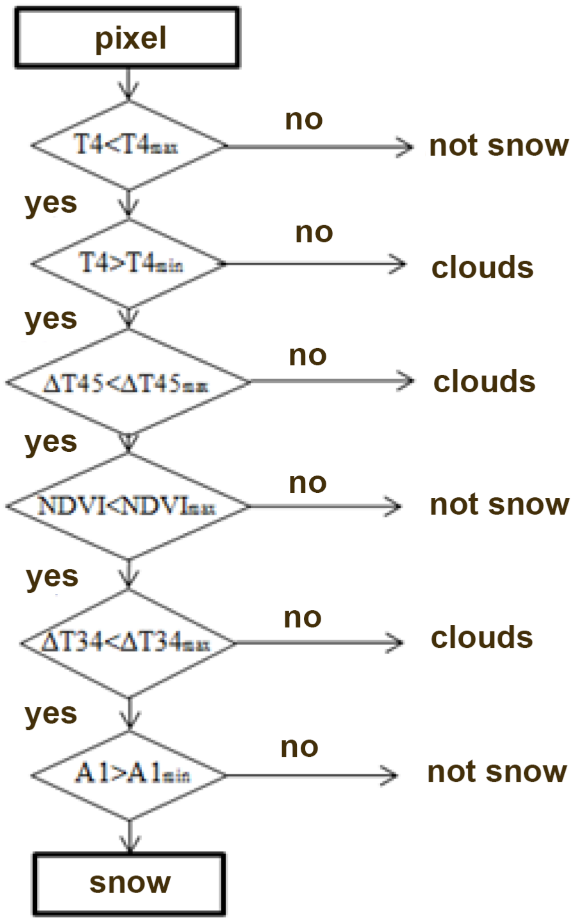

Fig. 1. Algorithm for detecting snow cover with the application of AVHRR [6] data.

3 and 4 T34, albedo (R) in channel 1 A1. The threshold values were obtained empirically only for one region (Eastern Canada) and for the time of year – early spring.

The high reliability of the results can be noted: the probability of the correct detection of snow reaches 97%. The snow mask is verified with the implementation of a large amount of ground data. Yet, the authors themselves position their algorithm as a regional one; the threshold levels are determined and work correctly solely for one region and one time of year.

The algorithm for generating a snow mask using MODIS/Terra, Aqua data is also based on constant thresholds [7, 10]. The algorithm employs NDSI, constant threshold values of reflectance in channel 2 (near IR) and reflectance in channel 4 (green). Pixels, in which NDSI values exceed 0.4, most likely, belong to the class of snow. If reflectance in channel 2 (near IR-range) exceeds 11% and reflectance in channel 4 (green) exceeds 10%, then the pixel is defined as snow with a probability of 100%.

Moreover, threshold values of the Normalized Difference Vegetation Index (NDVI) are used for forest-covered territories because the values of NDSI are lower for forest areas in comparison to those of a surface without vegetation.

Figure 2 gives a scattergram [5] of the distribution of R-values in channels 0.6 µm and 1.6 µm of AVHRR/NOAA-17 [11] obtained for the survey scene over the Alps. An open surface (clear), snow and clouds (cloudy) are present in the scene.

Mixed cells are present at the boundaries dividing the clusters of the abovementioned three types of surfaces in the scattergram.

The cell indicated by a yellow arrow is given as an example of such a situation: out of six points in a cell, three correspond to cloudiness, two – to an open surface and one – to snow cover. The sections of the image corresponding to the pixels in the mixed cell can be characterized as cloudless only with a probability of 50%. Note that the arrangement of clusters corresponding to the three types of surfaces (clouds, snow and open surface) indicates that any threshold values of the reflectance in the 0.6 µm and 1.6 µm will inevitably lead both to false alarms (commission errors) and gaps (omission errors) in the masks of snow or cloud cover.

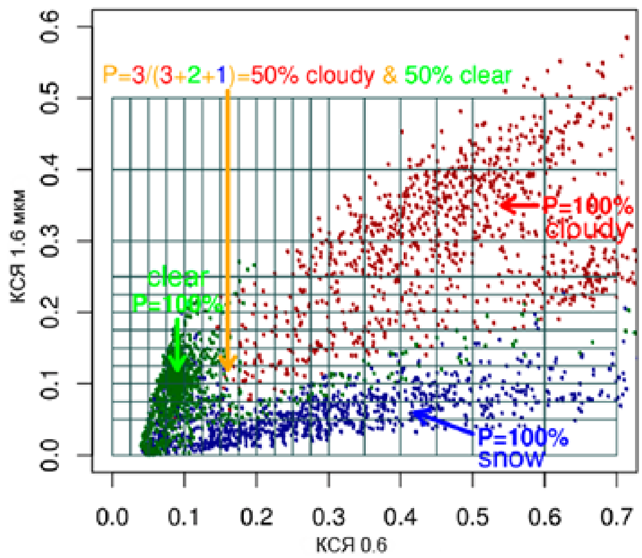

Fig. 2. Scattergram of the distribution of reflectance values in channels 1 and 3a of AVHRR/NOAA17 for various types of underlying surfaces according to a survey of the Alps [5].
* (clear) P – probability of the correct recognition of surface type.

Currently, practically all algorithms of snow mask generation use constant threshold values of reflectance, NDSI and radiation temperatures. The implementation of the abovementioned algorithms based on constant-threshold values on a global scale, Russia included, is complicated for the following reasons:

– thresholds are inconsistent and should change depending on the time of year;

– in most algorithms, thresholds are applicable only to a certain territory and their use for another territory leads to a noticeable decrease in reliability.

In addition, it should be noted that constant thresholds lead to the appearance of errors of the first and second kind, i.e. to gaps and false alarms. As a rule, errors occur at the boundaries of objects belonging to different types, which are characterized by a significant spread in R-values and radiation temperature values, for example, snow and ice inclusions in bare soil. The presence of errors is typical for any algorithm of snow and cloud mask formation but the use of constant thresholds exacerbates the situation. The algorithm set forth in the present paper for building masks of snow and cloud cover, not dependent on the time of year and territory, is primarily intended for providing exposure calculations performed by the satellite imagery planning complex. Maps of the snow and cloud covers are generated using MSU-MR/Meteor-M No. 2 data, which is received and processed on a daily basis by the Operator of Russian ERS space systems.

The main characteristics of the MSU-MR/Meteor-M No. 2 are given in Table 1. The same table also shows principal characteristics of the AVHRR, which is the foreign counterpart of the MSU-MR.

The initial data for the algorithm for detecting snow and cloud covers was the data of a daily survey of the MSU-MR/Meteor-M No. 2 of the territories of Canada, Russia and Europe obtained from 2015 to 2018. In total, 459 survey route fragments were used. The distribution of routes according to season is given in Table 2.

Table 2. Distribution of routes by season of the year and by region

	Number of routes			
Season of the year	Canada	Europe and the European part of Russia	Siberia and the Russian Far East	Total
Winter	27	28	9	64
Spring	43	32	29	104
Summer	39	24	143	206
Fall	30	46	9	85
Total	139	130	190	459

The coverage of the territory of Russia in the Far East and Eastern Siberia as well the survey of the territory of Canada are presented in Figure 3 in the form of overview images plotted on a map.

At the pre-processing stage, absolute calibration of MSU-MR data was performed, where the normalized digital readings were converted into physical quantities: into reflectance values in three short-wavelength channels and into values of radiation temperature in three long-wavelength channels.

Table 1. Main characteristics of MSU-MR / Meteor-M No. 2 and AVHRR

	MSU-MR		AVHRR	
Number of spectral channels	6		5 (working simultaneously)	
Spectral ranges	channel 1 channel 2 channel 3 channel 4 channel 5 channel 6	0.50 – 0.70 μm 0,70 – 1.10 μm 1.60 – 1.80 μm 3.50 – 4.10 μm 10.50 – 11.50 μm 11.50 – 12.50 μm	channel 1 channel 2 channel 3a channel 3b channel 4 channel 5	0.58 – 0.68 μm 0.725 – 1.10 μm 1.58 – 1.64 μm 3.55 – 3.93 μm 10.30 – 11.30 μm 11.50 – 12.50 μm
Swath, km	2800		2900	
Spatial resolution, km	1.0		1.1	

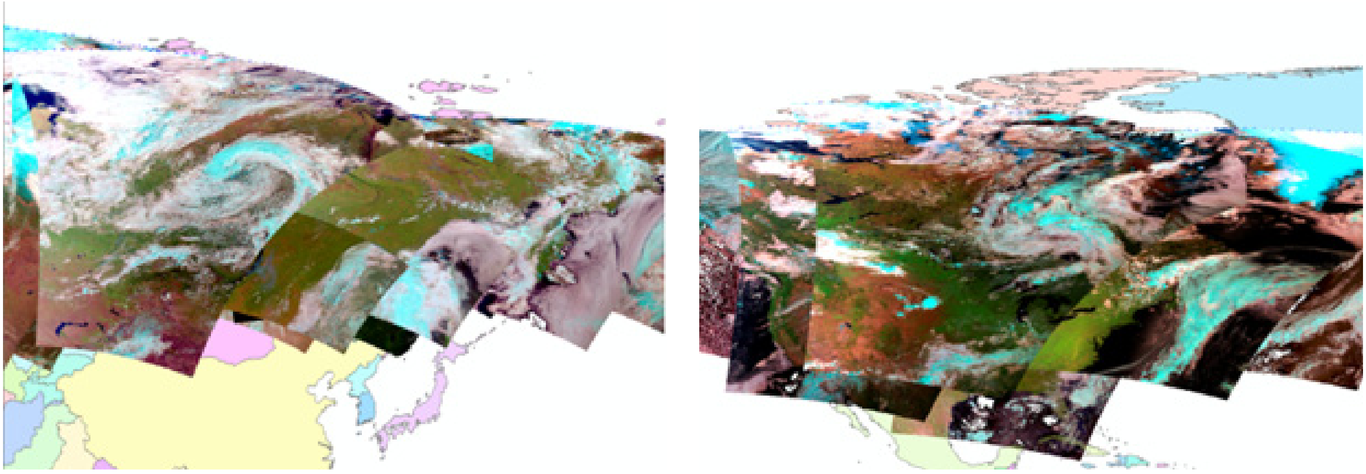

Fig. 3. Scheme of coverage by MSU-MR/Meteor-M No. 2 data of the territories of Eastern Siberia, Russian Far East (left) and Canada (right).

At the first stage, 17 survey routes were selected where all three types of surfaces are present: snow, clouds, "land" (in the given context, "land" means forest, sand and soil). The total area of test routes in the samples exceeds 130 million km^2. Areas known to belong to the each of the three surface types in every one of the seventeen routes are visually identified and outlined. The total area of the sampled territories attributable to clouds amounted to over 10 million km^2, the area of the sampled territories with snow cover was over 1 million km^2, the area of the sampled "land" – more than 500 000 km^2.

Figure 4 gives an example illustrating the result of this work: areas covered by clouds are marked by red contours; cloudless snow-covered areas are given with blue contours; open surface areas with "land" without snow and clouds – with green contours.

Data from MSU-MR measurements for the given areas were used to analyze the separability of the three surface types.

Considering that the most informative indicator for snow recognition is the NDSI, histograms of NDSI value distribution in the selected areas were built. In Figure 5, lines in shades of green represent NDSI histograms for "land"; red and lilac lines represent the NDSI values for clouds and blue, dark blue lines represent the NDSI histograms for snow. Histograms in Figure 5 are based on data from a survey conducted over a period of five days in May of 2016 over the territory of Canada.

According to the relative position of the histograms in Figure 5, the threshold value of NDSI = 0.4 (precisely this value of the NDSI index is used by the authors [7] when detecting the snow cover using MODIS data) allows

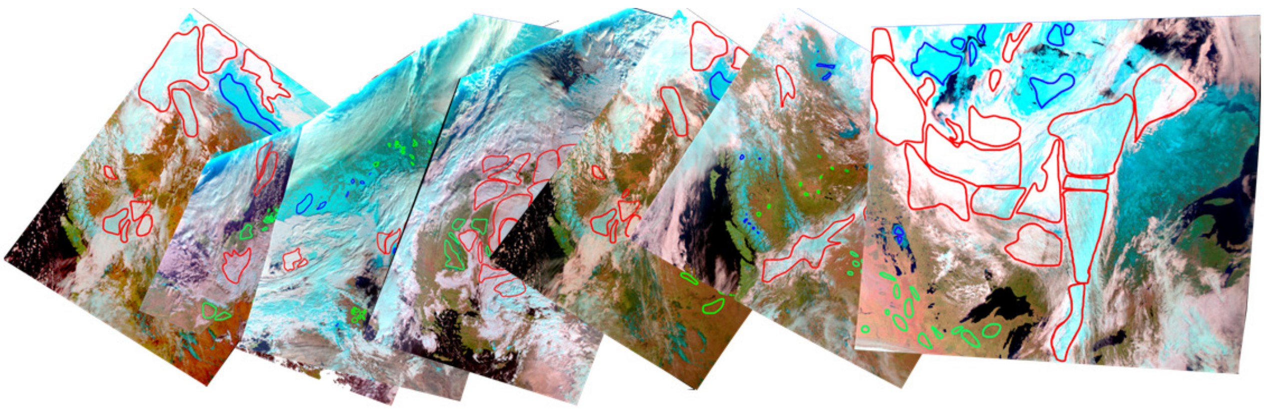

Fig. 4. Highlighting territories belonging to three types of surface types in images obtained in the period from autumn 2016 to spring 2017.

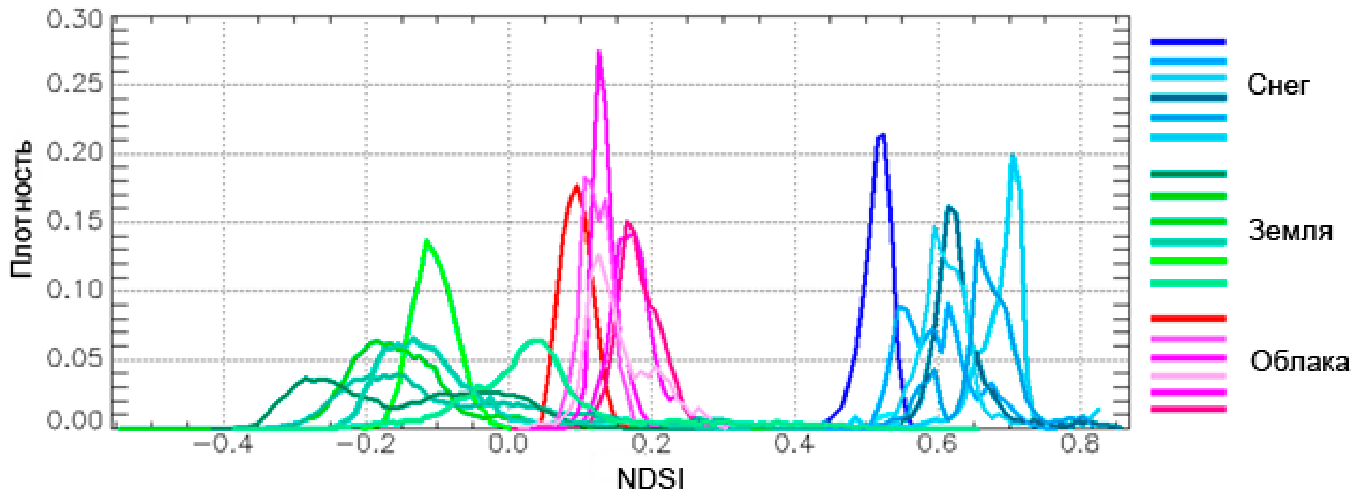

Fig. 5. Distribution histograms for routes over the territory of Canada.

to reliably discriminate areas containing snow from areas containing clouds and "land". Yet, no threshold value of NDSI provides a reliable differentiation between clouds and "land".

The next stage of the analysis consisted in building scattergrams for two indicators: NDSI and NDVI. Figure 6 demonstrates a scattergram of the distribution of NDSI-NDVI values for the same data sets as in Figure 5 obtained over the territory of Canada.

The distribution density of the pairs of NDSI-NDVI values is presented in the rainbow color palette: red corresponds to the highest frequency of occurrence of value pairs; yellow – to a lower frequency, blue and black – to the lowest occurrence frequency.

The scattergram in Figure 6 allows us to conclude that it is possible to reliably separate areas corresponding to snow and areas corresponding to "land" in the space of two indicators NDSI–NDVI. For this purpose, it is sufficient to determine a variable threshold, which can be represented as a function y=x. The graph of this function reliably cuts off snow from "land" but practically divides the cluster of values corresponding to clouds in half. Thus, in the space of two indicators – NDSI–NDVI even

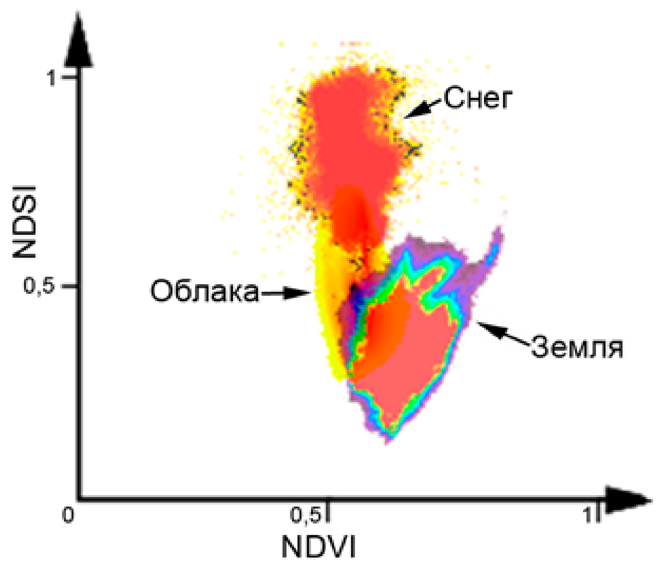

Fig. 6. Scattergram of the distribution of values in the NDSI-NDVI space for the selected areas corresponding to three surface types: cloudiness, snow, land – for five survey routes over the territory of Canada.

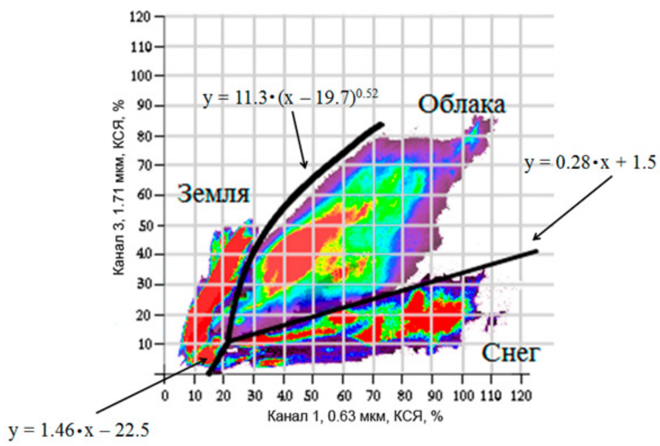

Fig. 7. Scattergram of the distribution of reflectance in channels 1 and 3 of MSU-MR/ Meteor-M No. 2.

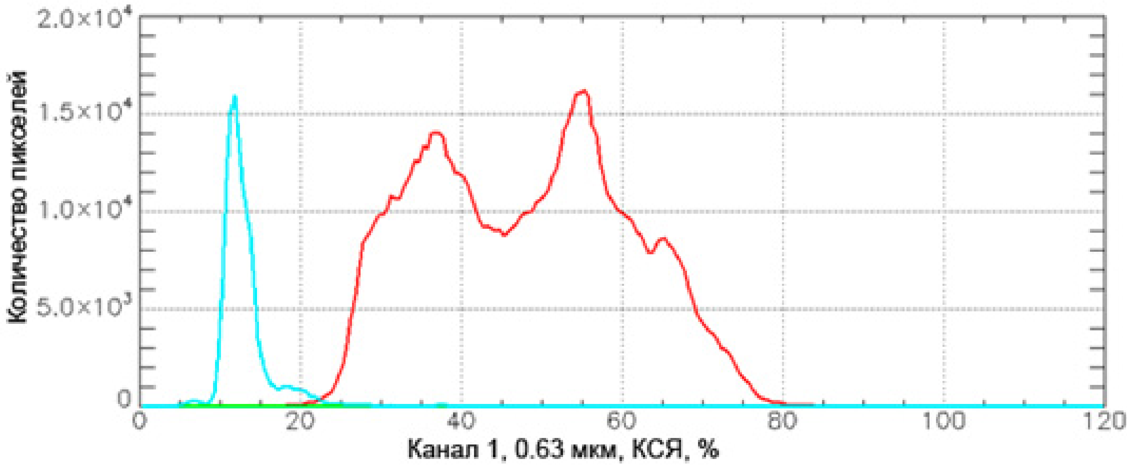

Fig. 8. Section of histogram in channel 1 (0.63 μm) within the limits of albedo values from 65% to 70%.

a variable threshold of the form y = x does not permit to solve the problem of reliably separating snow, cloudiness and an open surface completely.

Nevertheless, a more detailed study of the spectral properties of "land", clouds, snow with the use of all of the channels of MSU-MR allowed us to identify the possibility of their separation in the space of two indicators: reflectance, % (albedo) in channel 3 (SWIR-1, 1.7 μm) and reflectance, % in channel 1 (green, 0.63 μm).

Figure 7 shows a scattergram of the distribution of the indicated R-values for the previously selected areas (plots of "land") of land, cloudiness, and snow. Yet, the separation must be performed strictly with the use of variable thresholds; constant thresholds will not solve the problem. Note that the idea of the possibility of such separation of classes also arises during the analysis of the scattergram given in Figure 2 [5].

It is necessary to note that some R-values, % in channel 1 (0.63 μm), corresponding to bright objects exceed 100%. This is conditioned by the inaccurate calibration of the channels of the MSU-MR/Meteor –M No. 2 equipment noted in [12]. This also explains the presence of NDSI values exceeding 1 in Figure 6. Yet, it should be borne in mind that the inaccuracy of the absolute calibration does not affect either the algorithm or the result – the mask of cloud cover and mask of snow cover.

Here, as in Figure 6, the density of the distribution of R-values in 1.7 μm channel – R-values in channel 0.63 μm is given in the "rainbow" color palette (rainbow, ENVI environment)

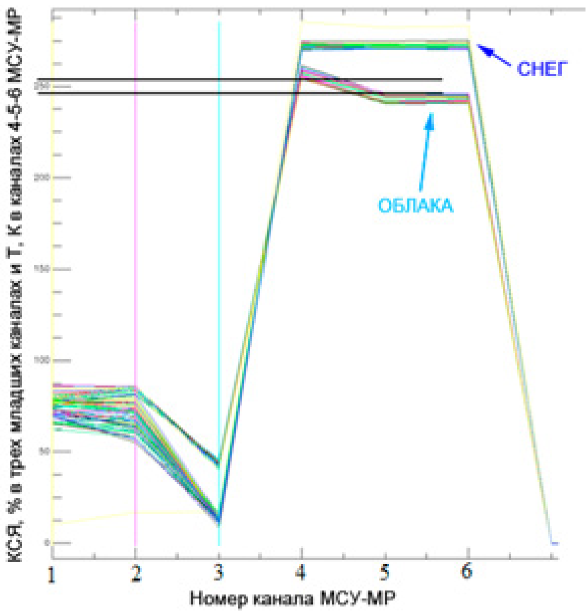

Fig. 9. Spectral images of objects pertaining to clouds or snow: difference in radiation temperatures in channels 4 and 5 of cloudy objects exceeds 3 K.

Variable threshold values are given in the form of functions y = f(x), where x is the value of the reflectance, %, in channel 1 of the MSU-MR (0.6 μm) and y is the value of reflectance, %, in channel 3 of the MSU-MR (1.7 μm). The graphs of the functions are presented in Figure 7 with thickened black lines. The expressions for function of the form y = f(x) are also given in Figure 7. Two functions out of three are represented as a linear function: $y = a \cdot x + b$; the third variable threshold is given in the form of a power function: $y = a \times (x+b)^c$.

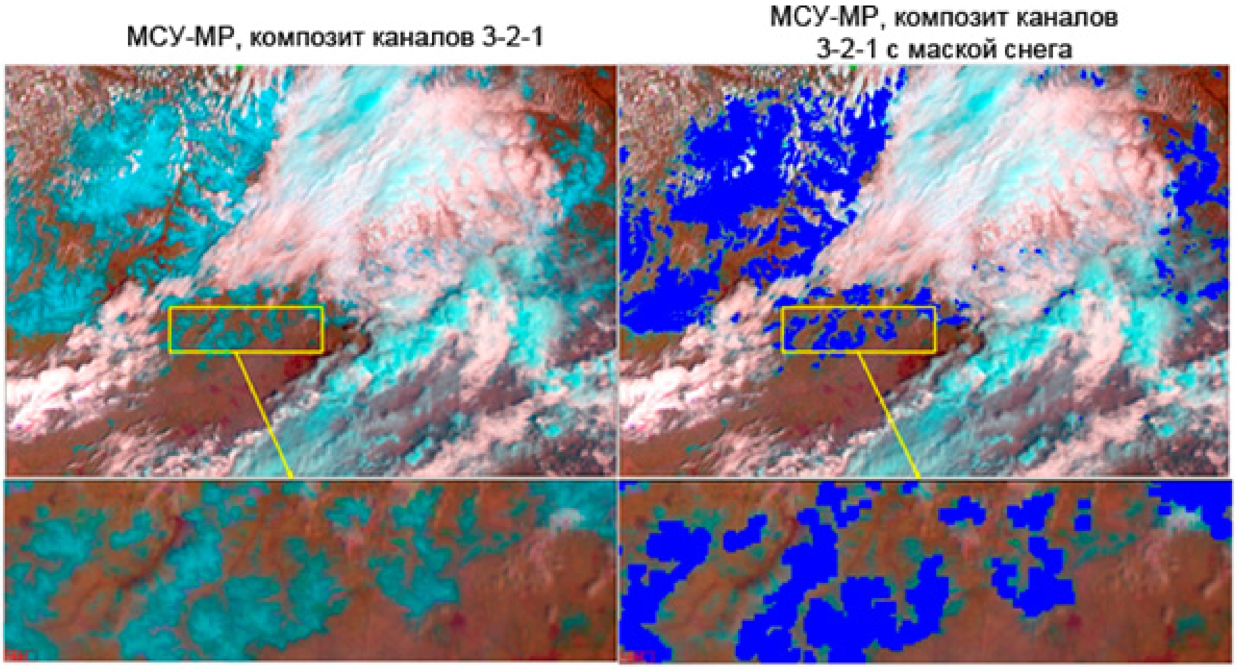

Fig. 10. Russian Far East, May 18, 2016, snow cover mask.

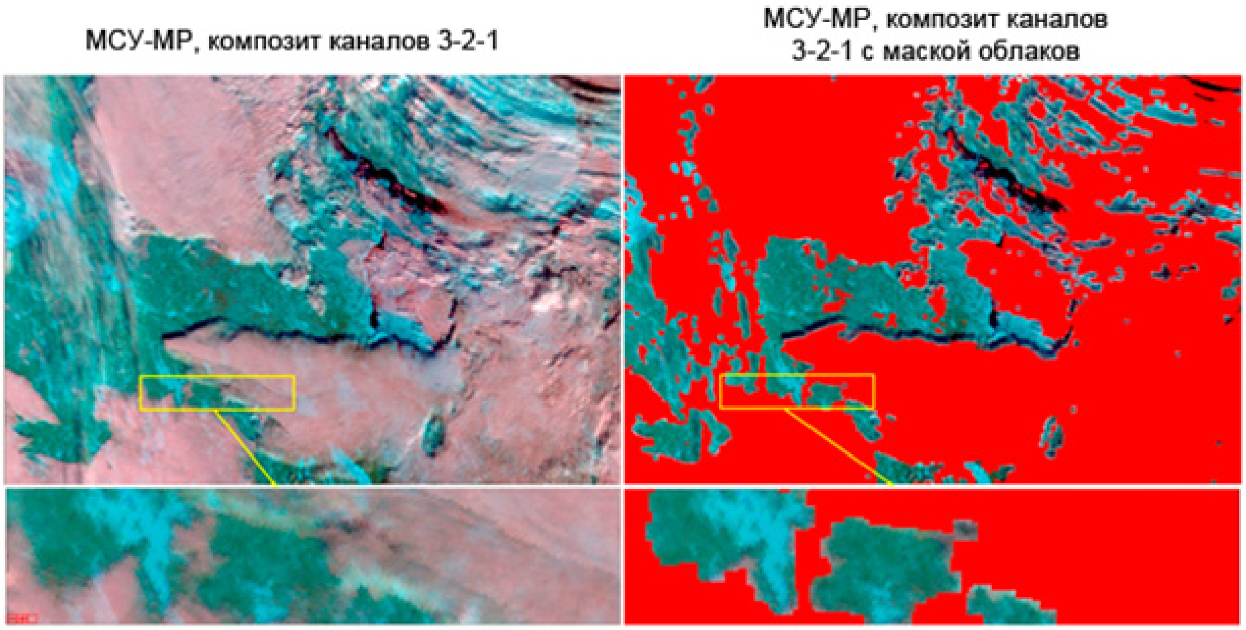

Fig. 11. European territory of Russia, February 27, 2017, cloud cover mask.

The evaluation of parameters a, b and c of variable threshold functions was performed with the help of the operation of equalizing the minimum standard error for a set of points, which is a set of particular threshold values that separate three types of surfaces. Particular threshold values were determined as follows. The entire space of the scattergram was divided along the x-axis into sections with a width of 5% in the range of low R-values and 10% – in the range of high R-values; for every segment with a width of 5% or 10% particular one-dimensional histograms were built. As an example, Figure 8 shows the particular histograms (land, snow, clouds) for the scattergram slice for R-values in channel 0.63 μm from 65% to 70%.

The middle parts of the sections, which the entire range of possible R-values was divided into in the 0.6 μm channel along the x-axis of the scattergram given in Figure 7, correspond to the x coordinates of points included in the set of particular threshold values. The y coordinates of the points in the set of threshold values were determined as R-values in the 1.7 μm channel, for which there is an intersection of particular histograms. For example, according to Figure 8, the particular threshold value for the range of R-values in the 0.63 μm from 65% to 70%, which discriminates snow from clouds, has the following coordinates: x = 67.5%, y = 22.8%.

In the process of algorithm validation, types of underlying surfaces were discovered, for which the application of additional conditions is required. Such objects include, for example, "land" with thin snow, which occurs, in particular, in late fall. Snow is classified erroneously as clouds on such a surface. The additional condition for correcting the error consists in the analysis of the values of the difference in radiation temperatures in the fourth and fifth channels of the MSU-MR: objects with a difference exceeding 3 K (Fig. 9) can be classified with confidence as clouds.

The variable threshold algorithm with an additional verification for early winter formed based on the data from 17 surveys of various territories was validated using survey data from Eastern Siberia, Russian Far East, the European territory of Russia as well as on Canada survey routes.

Testing confirmed the efficiency of the algorithm. The most important positive results are: 1) independence of variable thresholds from the time of year and 2) independence from the region where the survey is performed.

As an example, Figures 10 – 11 demonstrate the results of algorithm operation for two survey routes of the MSU-MR. Fig. 10 shows the Russian Far East in spring of 2016 and the mask of snow cover; Fig. 11 gives the European part of Russia in winter of 2017 and the cloud cover mask.

Note that the selected threshold values depend on the specific absolute calibration of the equipment. In order to maintain the correctness of the results over time or in case of a launch of a new SC, it is necessary to recalculate the coefficients of threshold functions or to take measures to ensure the constancy of the absolute radiometric calibration of MSU-MR. The latter, however, is true for any ERS data processing product.

It should also be noted that the developed algorithm of building snow and cloud masks does not provide pixel accuracy corresponding to the resolution of MSU-MR images of 1000 m. This is not conditioned by a peculiarity of the proposed algorithm but this is due to the general problem of surface classification: in transition zones – at the border, which divides objects of various types in the image, the probability of detecting objects of one type is reduced. This is caused by the simultaneous presence of signals incoming from objects of both types in the pixels of the given zone. Yet, it should be borne in mind that the snow and cloud mask generated with the help of the given algorithm is intended for use as a constituent part of the information base of the planning complex, in which data is given on a global scale (resolution – worse than 1 km). Consequently, the proposed algorithm ensures the generation of a snow mask and cloud mask, which are quite acceptable for planning (and processing) satellite surveys. The probability of detecting areal objects is close to 95 – 100%.

Conclusion

An algorithm is proposed for creating masks of snow and cloud cover using MSU-MR/Meteor-M data, which are a part of the planning complex for the target use of the Russian orbital constellation of ERS satellite and for processing the obtained data. The algorithm employs the values of the reflectance in channels 1 (green, 0.63 μm) and 3 (SWIR-1, 1.6 μm) of the MSU-MR. The significant difference of the present algorithm from analogues is the divergence from the practice of using constant thresholds. An analysis conducted on an extensive test set of source data demonstrated that the variable thresholds, which were determined by the present study, do not depend on the time of year or geographic location of the territory being surveyed.

Considering the continuous nature of MSU-MR surveys, the developed algorithm is capable of providing maps of snow cover and clouds in automatic mode with an update frequency of 2-3 days.

In the future, the introduction of the proposed algorithm in terms of snow cover mask formation directly into the technological complex of survey planning is anticipated. In addition, the cloud mask may be used to automate the process of searching for cloudless routes in archives of ERS data in accordance with consumer requests.

References

1. Gorbunov A.V., Il'ina I.Yu., Saul'skiy V.K. Sostoyaniye i perspektivy razvitiya kosmicheskikh kompleksov “Kanopus-V” i “Meteor-M” [State and perspectives of space complexes “Kanopus-V” and “Meteor-M” development]. *Raketno-kosmicheskoye priborostroyeniye i informatsionnyye sistemy* [Rocket-Space Device Engineering and Information Systems], Vol. 2, No. 4, 2015, pp. 14–19. (in Russian)
2. Stowe L.L., Jacobowitz H., Ohring G., R.K. Knapp, Nalli N.R. The Advanced Very High Resolution Radiometer (AVHRR) Pathfinder Atmosphere (PATMOS) Climate Dataset: Initial Analyses and Evaluations. *Journal of Climate*, Vol. 15, No. 11, June 2002, pp. 1243–1260.
3. *Portal distantsionnogo zondirovaniya* [Worldview Earth data]. Available at: https://worldview.earthdata.nasa.gov/ (accessed 23 September 2018). (in Russian)
4. Romanov P. Gutman G. Csisar I. Automated monitoring of snow cover over North America with multispectral satellite data. *Journal of Applied Meteorology*, Vol. 39, 2000, pp. 1866–1880.
5. Musial J.P., Hüsler F. Probabilistic approach to cloud and snow detection on Advanced Very High Resolution Radiometer (AVHRR) imagery. *Atmospheric Measurement Techniques*, 7, 2014, pp. 799–822.
6. Chokmani K., Bernier M., Royer A. A Merging Algorithm for Regional Snow Mapping over Eastern Canada from AVHRR and SSM/I Data. *Remote Sensing*, 5, 2013, pp. 5463–5487.
7. Hall D.K., Barton J.S. *Algorithm Theoretical Basis Document (ATBD) for the MODIS Snow and Sea Ice-Mapping Algorithms.* Available at: http://modis-snow-ice.gsfc.nasa.gov (accessed 04 April 2018).
8. Boschetti M., Nutini F., Manfron G., Brivio P.A., Nelson A.D. Comparative Analysis of Normalised Difference Spectral Indices Derived from MODIS for Detecting Surface Water in Flooded Rice Cropping Systems. *PLoS ONE*, Vol. 9, No. 2, 2014. Available at: https://www.researchgate.net/publication/260447511_Comparative_Analysis_of_Normalised_Difference_Spectral_Indices_Derived_from_MODIS_for_Detecting_Surface_Water_in_Flooded_Rice_Cropping_Systems (accessed 06 June 2019).
9. Gandhi M.G., Parthiban S., Thummalu N., Christy A. Vegetation Change Detection Using Remote Sensing and Gis – A Case Study of Vellore District. *Procedia Computer Science*, Vol. 57, 2015, pp. 1199–1210.
10. Xiong X., Barnes W., An overview of MODIS radiometric calibration and characterization. *Atmospheric Environment*, Vol. 37, No. 17, June 2003, pp. 2403–2412.
11. Ignatov A., Sapper J., Laszlo I., Nalli N., Kidwell K. Operational Aerosol Observations (AEROBS) from AVHRR/3 On Board NOAA-KLM Satellites. *Journal of atmosphere and Oceanic Technology*, Vol. 21, No. 1, January 2004, pp. 3–26.
12. Filei A.A., Rublev A.N., Kiseleva Yu.V. Otsenka stabil'nosti radiometricheskoy kalibrovki korotkovolnovykh kanalov mnogokanal'nogo sputnikovogo ustroystva KA “Meteor-M” No. 2 [Estimation of the stability of radiometric calibration of Multi-Channel Scanning Unit shortwave channels on board Meteor-M No. 2]. *Sovremennyye problemy distantsionnogo zondirovaniya Zemli iz kosmosa* [Current problems in remote sensing of the Earth from space], Vol. 15, No. 42018, pp. 71–77. (in Russian)